A Medium Voltage AC and DC Distributed Power Generation Testbed Deploying Transient Loads

A N Johnston*, D A Wetz*, G K Turner*, Z R Bailey*, D A Dodson*, B J McRee*, and J M Heinzel+

*Univ. of Texas at Arlington (UTA), Arlington, TX USA
+Naval Surface Warfare Center - Philadelphia, Philadelphia, PA USA
* Corresponding Author. Email: wetz@uta.edu

Synopsis

Microgrids have been studied considerably over the last decade. They are being uniquely designed and controlled in a variety of applications to supply countless different loads, many of which may operate in a transient manner. Given their isolated nature, ships are often treated as microgrids allowing much of the same theory to apply. Historically, both electric grids and ships have relied upon fossil fuel powered motors to spin generators that source the electric power they need. Microgrids can deploy a host of different distributed generation sources that are interconnected and controlled in real time to improve overall grid reliability and redundancy. The use of medium-voltage-direct-current (MVDC) power distribution is one possible solution to minimize power loss in the conductors and to reduce the power conversion requirement when high voltage loads are present. The non-continuous operation of loads may introduce harmonics into the power system that severely impact power quality. Avoiding this is critical and more must be understood for successful mitigation. Model development and validation is critical for successfully deploying new architectures and control strategies. To study the reliable operation and control of such a power system, as well as to validate the models being developed, the Pulsed Power and Energy Laboratory (PPEL) at the University of Texas at Arlington (UTA) has designed and installed a testbed that can be used to study a small microgrid deploying transient loads. The testbed, operating at power levels higher than 300 kW, utilizes distributed AC and DC power sources and loads operating at the 480 VAC, 4160 VAC, 1 kVDC, 6 kVDC, and 12 kVDC, respectively. The testbed is being virtually extended utilizing a hardware in the loop (HIL) simulator. This paper will discuss the design of the testbed, the test plan methodology, and the results collected so far.

Keywords: Microgrid; Medium-Voltage Power Distribution; Power System Control; Power Electronics; Energy Storage

1. Introduction: Moving away from mechanical propulsion

Future ships will demand more from their electrical power sources than ever before [1-4]. This stems from the desire to install electrical propulsion systems as well as transiently operated loads [4-6] that will suddenly introduce unexpected periods of elevated and decreased load, respectively. This operation is tremendously hard on traditional diesel and gas-turbine engine-generator sets and can significantly affect power quality [4-5]. It has been proposed that an interconnected network of distributed generation sources, made up of both AC and DC sources, can be employed to maintain power quality [5]. Interconnection of the different sources can be achieved in many ways. One is the that proposed by Doerry [7], seen in Figure 1, in which the power system is broken up into zones, each of which has its own sources, loads, and power electronic converters, respectively. Interconnection of multiple zones is achieved using a dual medium voltage (MV) DC bus and bi-directional power converters that allow each zone to share power amongst them. Monitoring of power flow throughout the power system is critical and so is having a control system that can respond to dynamic changes quickly. Energy storage plays a vital role in this type of power system architecture due to its ability to buffer AC sources during both high and low load activity. A battery's ability to both supply and absorb high peak power is a very important benefit, though symmetric operation is seldomly recommended. This makes distributed control even more critical.

These are not new challenges, as they are very similar to the ones faced every day as power systems engineers try to integrate batteries, solar panels, and wind turbines onto the already existing electrical grid, either in homes or in the larger distribution network. What makes it challenging aboard a ship is the lack of stiffness typically found in traditional power sources under high load and the transient nature of the loads that may need to be supplied. Special attention and research is needed to understand how to overcome these challenges. The University of Texas at Arlington's (UTA's) Pulsed Power and Energy Laboratory (PPEL) has experience supporting research in areas related to integrating and controlling energy storage within future shipboard power systems. In addition to completing several studies at the cell and module levels [6,8-9], respectively, UTA has designed, constructed, and demonstrated the transient operation of two 1000 V batteries at power levels greater

than 250 kW [10-11]. In addition to studying the independent operation of those batteries, UTA has designed, constructed, and evaluated an autonomous hybrid energy storage module (HESM) using commercial off the shelf (COTS) components [5,11-13]. UTA's HESM utilizes actively controlled power electronics to regulate the power flow of its lithium-ion battery and ultracapacitor energy storage autonomously depending on load detected and deviation monitored on is DC output bus. The HESM has been integrated with hardware in the loop (HIL) emulated AC sources as well COTS gasoline powered generators [5,14]. Experiments performed with these sources has demonstrated the HESM's ability to buffer transient loads and maintain AC power quality.
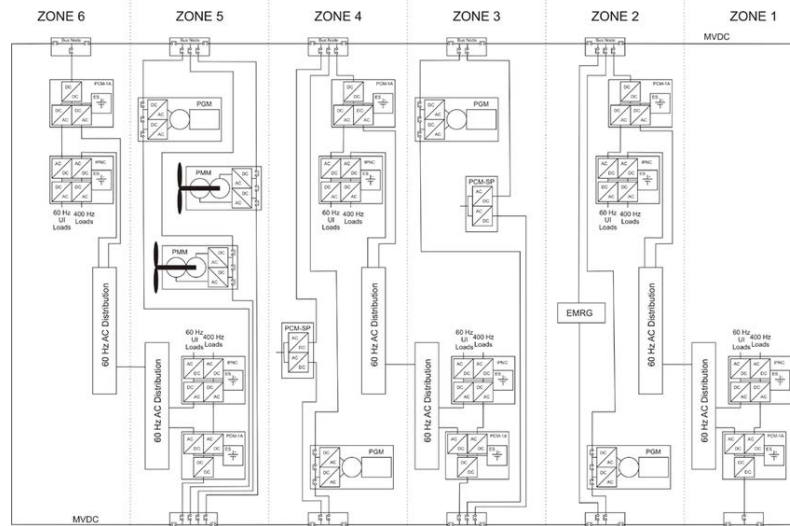
Figure 1: Doerry's MVDC reference architecture [1].

The advent of using testbeds to illustrate, model, and preliminarily implement future smart microgrids has been explored a few times previously. One of which was conducted at the City College of New York but only used DC components and used minimal COTS components and another is the CERTS microgrid in Columbus, OH in which is designed to create a system of steps to remove a microgrid from the overall power grid [15,16]. These both work more in the consumer market and focus less on the specificity of the transient type loading that would occur in a shipboard power system. As such, the PPEL hope to shine additional light on these transient problems in a medium power zonal architecture.

This report will discuss the design, development, and commissioning of a MV DC/AC testbed. The testbed, referred to as the Intelligent Distributed Energy Analysis Laboratory (IDEAL) is installed on the UTA campus and has 1 kVDC, 6 kVDC, 12 kVDC, 480 VAC, and 4160 VAC sources and loads, respectively, installed. Grid-tied and rotating machine AC sources are installed along with any one of the 1 kVDC batteries discussed earlier. The testbed is monitored and controlled in real time using a National Instruments (NI) data acquisition and control system. The NI hardware is interfaced with an OPAL-RT hardware in the loop (HIL) system that is used for source and/or load emulation as well as additional control as needed. Currently, the testbed is extended into a very simplified five-zone shipboard system, modeled off the type of architecture shown in Figure 1, using the OPAL-RT. The testbed is being used to study the design and control of multiple AC/DC sources, their power quality when they are transiently loaded, and the interconnection challenges that such a power system faces. Though it will not be discussed in detail here, the testbed is being modeled using Simulink and the testbed is being used to validate those models. How well a COTS product needs to be understood to obtain an accurate model is still in question and is a focus of the work performed here. The design, construction, and commissioning of the testbed will be discussed in later sections. A possible control strategy will be highlighted and its application to the virtual extension will be presented.

2. IDEAL Experimental Testbed

The design of future shipboard power systems will be impossible without validated simulation models. UTA has installed a unique testbed, shown schematically in Figure 2, to be used in support model development, verification, and validation. The testbed shown in Figure 2 is being used to study and validate distributed power system architectures and control strategies. An Opal-RT Hardware in the Loop (HIL) system is being used to extend the hardware virtually and to emulate controllers and other hardware not possessed in the lab. The next several sections of this paper, discuss the testbed hardware and its capabilities.

In Figure 2, it is shown how the testbed converts AC power to DC power to drive 6 kV and 12 kV MVDC loads, respectively, and how a 1 kVDC energy storage device is used to supply its own load or buffer the AC source. Also sourced is a 480 VAC load. In most cases, the testbed's primary source of power is the 150 kW electrical motor-generator (M-G) set, though the installation is such that the electrical grid can be used to power all or some of the testbed as needed. Each individual testbed component will be discussed in the following subsections.
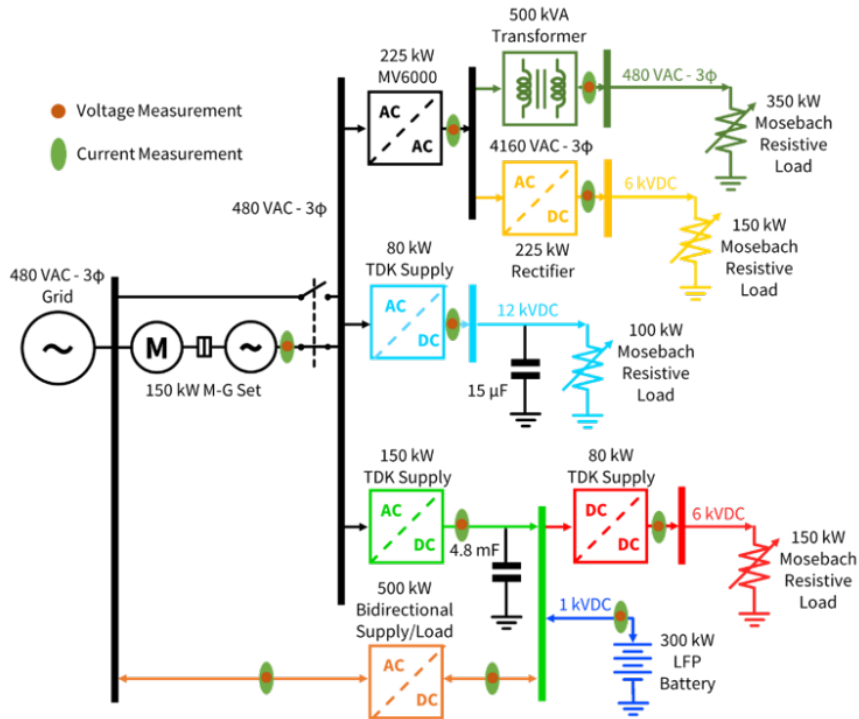
Figure 2: Electrical one-line diagram of the IDEAL MV DC/AC hardware testbed.

2.1. 150 kW KATO Electrical Motor – Generator (M-G) Set

On the left side of Figure 2, an electrical M-G set, seen photographically in Figure 3, acts as the primary source of three phase, 480 VAC power for the testbed. It utilizes a 300 HP four-pole induction motor to spin a four-pole synchronous generator at 1500 – 2000 RPM. The motor is spun using a variable frequency drive (VFD) that is supplied by a 480 VAC, 400 A electrical feed.

Figure 3: Photographs showing the M-G set (left) and internals of the control and VFD cabinets (right).

The generator is designed so that the amplitude of its output voltage and frequency can be adjusted remotely using two respective analog control signals. The output voltage is variable from -20% (384 VAC) to +20% (576 VAC) of the nominal 480 VAC using the 0 V – 10 V analog signal. The output frequency is adjustable from -17% (50 Hz) to +11% (67 Hz) of the nominal 60 Hz using a second 0 V – 10 V analog control signal. This

feature allows the generator's output to be modulated using a real time OPAL-RT hardware in the loop (HIL) simulation platform. This is desirable since the inherent electrical and mechanical properties of the M-G set do not directly match those of a fielded diesel or gas-turbine M-G set. Using validated Simulink models of fielded M-G sets, the KATO M-G set can be used as an amplifier of the OPAL-RT's simulation output. This type of configuration, one in which a simulated HIL model is amplified to emulate a component as shown in Figure 4, is referred to as Power HIL (PHIL).

In Figure 2, the M-G's output supplies three respective circuit branches off the 480 VAC point of common coupling (PCC). Those branches are into a 225 kW - 480 VAC to 4160 VAC, five level power electronic drive, a 80 kW – 480 VAC to 12 kVDC switch mode power supply, and a 150 kW – 480 VAC to 1.2 kVDC switch mode power supply, respectively. Each of these circuit branches will be described in the next few sub-sections.
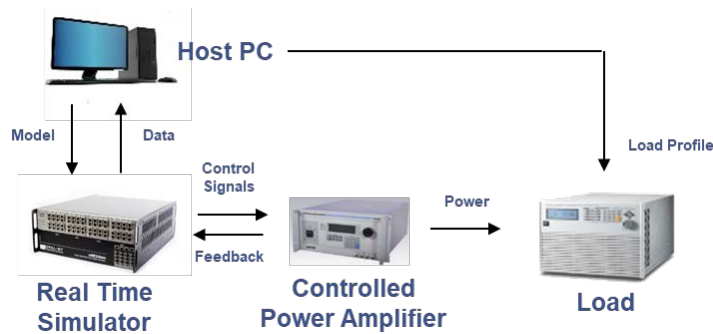
Figure 4: Simple schematic describing setup of power hardware in the loop.

2.2. GE MV6000 Power Electronic Drive

Working from the top down on the 480 VAC PCC in Figure 2., the first electrical load connected to PCC a 225 kW MV6000 power electronic drive, seen in the left side of Figure 5, that is manufactured by General Electric (GE) [17]. The M-G set is only capable of supplying 150 kW so the MV6000 alone can exceed that, not to mention all the other loads on the PCC. Caution in the overarching control system is given to ensure that the generator's power is never exceeded. The MV6000 is typically utilized in industry as a VFD for MV motors. A simple schematic of its internal operation is shown on the right side of Figure 5. Its input is an eighteen - phase shifting transformer that steps up 480 VAC to 4160 VAC, RMS. The eighteen phases are fed into a thirty-six-pulse diode rectifier that rectifies the secondary AC voltage to roughly 6 kVDC and that is placed onto a capacitive DC link. The DC link feeds a five - level IGBT inverter that generates a three - phase 4160 VAC output. The MV6000's output voltage and frequency are also able to be modulated using two respective 0 – 10 V analog signals supplied by the Opal-RT. The output voltage can be varied from 80% to 110% of its rated 4160 VAC output and its frequency can be varied from 50 Hz to 70 Hz, respectively. Because the MV6000 is a switch mode converter, the output does have a switching component to it that must be filtered for a true sinusoidal output to be obtained. The 4160 VAC source can supply two different circuit branches from its own respective PCC, discussed next.
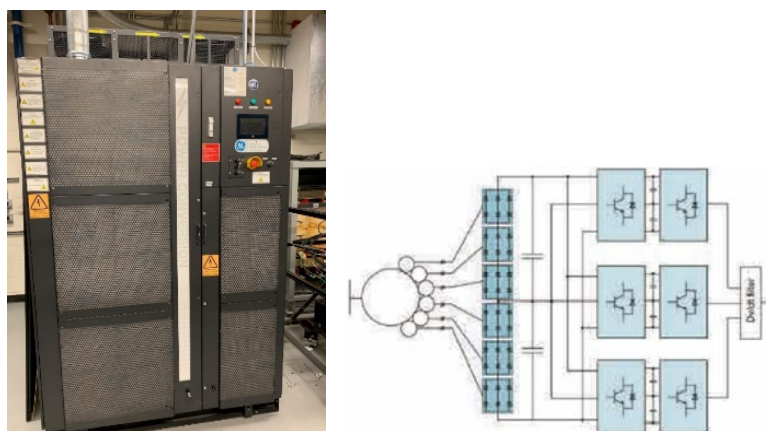
Figure 5: Photograph of the GE MV6000 power electronic drive (left) and simple schematic describing the internal operation of the MV6000 (right). First is the eighteen-phase step-up transformer, next is the thirty-six pulse diode rectifier that creates a 6 kVDC link, and finally there is a five-level IGBT inverter that creates the three phase 4160 VAC output [17].

2.3. 4160 to 480 VAC Step Down Transformer and 350 kW – 480 VAC Mosebach Electronic Load

One of the two respective electrical branches supplied by the 4160 VAC PCC is into a 500 kVA step-down transformer, seen in the left side of Figure 6, which converts the 4160 VAC to 480 VAC. A 350 kW - 480 VAC electronic load, seen on the right side of Figure 6, is connected at the output of the transformer that serves as either a base load or as a variable step load on the bus. The 480 VAC load, offered as a standard product from Mosebach, is purely resistive with 1 kW step resolution. The load steps are controlled using 24 V digital logic supplied by the NI control system. The variable step resolution allows the user to emulate the typical stepping on and off, respectively, of typical shipboard hotel loads.

Figure 6: Photograph of the 500 kVA - 4160 VAC / 480 VAC step down transformer installed in the laboratory (left) and of the Mosebach 350 kVA - 480 VAC resistive electronic load installed in the laboratory (right).

2.4. GE 18 Pulse Transformer, GE 36 Pulse Diode Rectifier, and Mosebach 6 kV Resistive Load Bank

The second electrical branch fed off the 4160 VAC PCC is into a GE eighteen - phase shifting transformer/rectifier, seen in Figure 7, that is identical to the one at the input to the MV6000. The only difference in this transformer from the one in the MV6000 is that its input rating is 4160 VAC, instead of 480 VAC, and it has a near unity gain. The output of the eighteen - phase transformer is rectified using the same type of thirty-six pulse diode rectifier that the MV6000 uses. It rectifies the AC input to roughly 6 kVDC. By using a multi-pulse rectifier in place of a simple three – phase rectifier, the ripple of the rectified DC voltage is reduced however as the results later will show, without a filter, it is still quite variable. The transformer and rectifier were procured from GE as piece parts that had to be integrated into a single package. A custom steel frame was designed that is on casters so that it can be moved around as needed. The rectifier, designed in three module blocks by GE, sits above the transformer on an isolated fiberglass reinforced frame.

Forced air cooling is needed to ensure the transformer and rectifier stay below their rated thermal limits during electrical operation. An air flow rate of 160 m^3/min is recommended to ensure safe operation. To achieve this, a 15 HP blower is used to force air through the transformer enclosure. The port used to push air into the enclosure is shown in the right image of Figure 7 and the 15 HP blower along with its associated variable frequency drive and braking resistor are shown in Figure 8. The transformer has integrated temperature diagnostics that are monitored by the NI control system to prevent overheating.

Figure 7: Photograph of the 225 kW, eighteen - phase transformer and thirty-six pulse AC/DC rectifier within the custom enclosure fabricated for safety and for forced air cooling. The transformer is below and the white rectifiers are seen above it.

Figure 8: Photograph of the 15 HP blow, variable frequency drive, and braking resistor used to apply forced air cooling to the 4160 VAC transformer and 4160 VAC/ 6 kVDC rectifier.

2.5. 6 and 12 kVDC Electrical Loads

The output of the 6 kV rectifier is fed into 6 kVDC resistive load, seen on the left side of Figure 9, fabricated by Mosebach. Two identical 6 kVDC loads were procured. Each load is comprised of three – 50 kW steps and each step is connected to the source through a single pole vacuum contactor manufactured by Ross Engineering, model hbdc51-no-40-2-0-bd. The contactors can switch up to 10 A at 50 kV and have an electrode life of roughly 50,000 switching cycles. The contactors are engaged using 24 V logic from the host controller and internal to the load is conversion of that digital signal to the 120 VAC that actuates the contactors. Though the loads are designed to have three 50 kW steps, the steps can be manually reconfigured into a few different power levels by altering the connections of the four independent resistive networks. A similar resistive load designed to load 100 kW at 12 kVDC was also procured, seen in the right side of Figure 9. It is made nearly the same way as the 6 kV loads, with approximately the same footprint, but it only has two – 50 kW steps installed that are each connected to the source using the same type of Ross relay.

Figure 9: Photograph of the two 6 kVDC – 150 kW resistive loads (left), and 12 kVDC – 100 kW resistive load (right).

2.6. 80 kW 480 VAC to 12 kVDC Programmable AC/DC Power Supply

The second load down on the 480 VAC PCC in Figure 2., is a 480 VAC to 12 kVDC switch mode power supply that is operable up to roughly 80 kW. The two – 12 kVDC liquid cooled supplies are shown photographically in the upper two slots of the rack seen in Figure 10. The two independent supplies operate in parallel using a master-slave configuration. The supplies are designed for use as capacitor chargers but are capable of being used as DC supplies if loaded with a capacitive buffer. A 15 µF capacitor is connected across their output to ensure there is always load for them to supply. The 12 kVDC power supply is current controlled remotely using an analog reference signal that is generated by the National Instruments (NI) LabVIEW controller that will be discussed in further detail later. The OPAL-RT controller can also be used as needed. Modulation of the current allows the power supply to emulate high voltage transient loads, as shown in the results section later. The 12 kV power supply is loaded using the 12 kVDC resistive load bank discussed previously.

Figure 10. Photograph showing the two – 40 kW power supplies used to convert 480 VAC to 12 kVDC (upper two supplies) and the three – 50 kW power supplies used to convert 480 VAC to 1.2 kVDC (lower three supplies).

2.7. 150 kW 480 VAC to 1.2 kVDC Programmable AC/DC Power Supply

The third electrical branch supplied off the 480 VAC PCC is into a liquid cooled, 150 kW DC/AC power supply, seen in Figure 10. The input to the supply is 480 VAC and its DC output is variable from 30 VDC to 1.2 kVDC. The power converter is assembled as three independent 50 kW supplies that operate in a master-slave configuration, like the 12 kVDC supplies discussed earlier. The 12 kVDC supply is also designed as a capacitor charger so it must always have a capacitive load connected. This is achieved by floating a 11 kV, 4.8 mF capacitor on its output. The supply's current or voltage, respectively, is modulated using 0 – 10 V analog signals supplied by the controller. In normal operation, the output current of the supply is remotely modulated and controlled using the overarching NI or OPAL-RT controller, respectively. This enables them to also be used to emulate other types of rectifier topologies or load profiles as needed. UTA has previously shown that when using accurate Simulink® models, HIL emulation is able to very accurately replicate experimental hardware that is not possessed [14,18].

2.8. 1 kVDC Lithium-Iron Phosphate Battery

The 1.2 kVDC power supply sources power onto a ~1 kVDC bus that is buffered using a high-power lithium-ion battery, seen in Figure 11. The battery is assembled using Saft VL30AFE cells and can load roughly 96 kW and source 250 kW continuously. The battery can source power onto the ~1 kVDC PCC or sink power from the AC source through the 1.2 kVDC power supply. When transient loads are sourced, the battery can augment the AC source to supply the load and when the load is inactive, the battery can load the AC source, allowing it to maintain a steady output power. This allows the AC source to maintain acceptable AC power quality during transient load operation. One intention of the testbed is to demonstrate the ability to maintain power quality in this type of operational scenario and to both develop and validate the overarching system controller needed to achieve this goal.
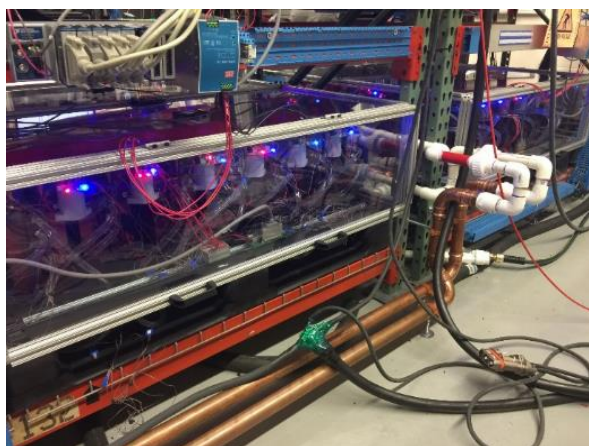
Figure 11. Photograph of the 1 kVDC LFP-LI battery during operation as indicated by the illumination of the many respective blue and red relay control board LEDs.

2.9. 1 kVDC – 6 kVDC Programmable Power Supply

The ~1 kVDC bus is loaded by two different branches. The first one is into a programmable DC/DC power supply. The supply has an input voltage ranging from 700 VDC to 1000 VDC and output voltage as high as 6 kVDC. The supply is like the ones shown in Figure 10. The power supply is nominally rated to supply roughly 54 kW to its load (though 80 kW is achievable for several minutes). This supply is also designed as a capacitive power supply though it is operated in a DC test mode. Its output current is similarly modulated using a 0 – 10 V analog signal from the NI or OPAL-RT controller. The output of the supply is loaded using the second 6 kVDC Mosebach resistive load already discussed earlier.

2.10. 1.2 kV Programmable Power Supply and Load

The second branch off the ~1 kVDC PCC is into a Chroma 17030 programmable cycler that can act as either programmable power supply or as a programmable load with ratings of 1.2 kVDC/ 700 ADC/ 500kW. The 17030 is regenerative and supplied by the building's main 480 VAC grid feed. It serves as a non-linear load on the ~1 kVDC bus and as a secondary power supply as needed. The cycler is controlled using Chroma's own software or using -10 – 10 V analog control signals in constant current (CC), constant voltage (CV), constant resistance (CR), and constant power (CP) modes of operation. The system has a slew rate of roughly 10 ms and is regenerative with the building's 480 VAC utility grid. A photograph of the cycler is shown in Figure 12.

Figure 12. Photograph of UTA's 1200V/700A/500kW Chroma 17030 cycler.

2.11. Data Acquisition, Hardware in the Loop (HIL), Overarching Control

For the controller and supporting control algorithms to work, the system needs to monitor states and react. The overarching control and data acquisition (DAQ) of the testbed is briefly discussed in the next few sections.

2.11.1 Voltage and Current Monitoring

AC and DC voltage and current measurements, respectively, are made throughout the testbed, as illustrated in Figure 2 with the orange and green circles. They are measured and digitized using multiple NI CompactDAQ (cDAQ) cards mounted in a few different NI cDAQ chassis. A NI PXI chassis, instrumented with several voltage measurement cards, and the OPAL-RT HIL system are also used for data acquisition and monitoring. A photograph of the shielded controls cabinet housing the cDAQs is shown in Figure 13 and one showing the PXI chassis and the OPAL-RT, respectively, is shown in Figure 14.

Figure 13: Cabinet housing the four NI cDAQ chassis providing overarching control of the different power supplies, Mosebach loads, MV6000, and M-G set.

The networked cDAQs and the OPAL-RT work together to provide real-time control of the hardware. Each system monitors voltage and current waveforms needed to make real time decisions. Network variables are used to share measurements across platforms. The sample rate varies across systems to optimize processing speed and resolution needed for testbed performance analysis. Nearly all current measurements are made using closed loop Hall Effect current sensors. The primary ones used are Harting 100 A and 300 A sensors that have a bandwidth of 50 kHz. Voltage measurements are made using a few different types of differential voltage probes. The first is a 1.4 kV - 25 MHz, differential voltage probe manufactured by Pico Technology (model TA057). The second is a 7.0 kV - 70 MHz, differential voltage probe also manufactured by Pico Technologies (model TA044). Thermal monitoring, which will not be elaborated here, is achieved using distributed thermocouples and an ODiSI fiber optic thermal sensing system [17].

Figure 14: Photograph of the NI PXI chassis and OPAL-RT, respectively.

2.11.2 User Interface and Virtual Extension

The hardware testbed is intended to emulate one zone of a multi-zonal shipboard power system [7]. The testbed is extended virtually using the OPAL-RT simulator. The eventual goal is to have a finely detailed shipboard power system model. As currently implemented, the extended model is kept very simple, shown in Figure 15. Four additional zones are made up using a few simple M-G sets, power electronic converters, and pulsed resistive loads. The extended five zone system has been validated, however, because the loads are so simple, this will not be discussed in more detail here. It is instead presented to inform of the path the research will be taking in the future.
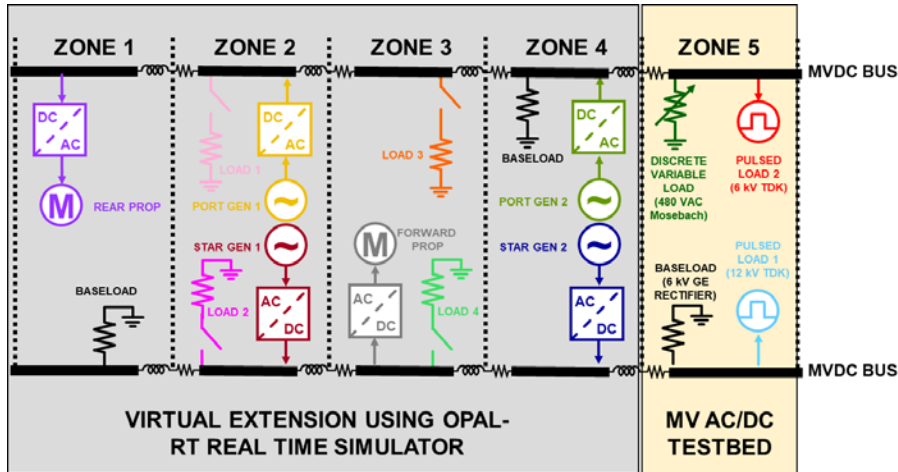
Figure 15: One-line diagram of the five-zone, OPAL-RT extended shipboard model.

The user controls the testbed via the control box shown in Figure 16. The box's functionality is described in Figure 17. The color-coded one-line diagrams in Figure 2 and Figure 15, respectively, describe what each button controls within the testbed.

Figure 16: Photograph of the user control box designed and developed for interfacing with the testbed.
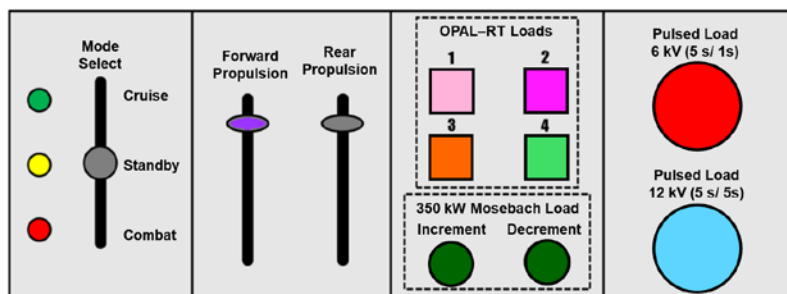
Figure 17: Diagram describing the functionality of the user control box in Figure 16.

On the left side is a three-position toggle switch that is used to adjust the slew rate of the propulsion motors within the OPAL-RT model and the setting is used by the control system to define how the system hardware setpoints are optimized. Moving to the right, there are two sliding potentiometers that control the propulsion motors in Zones 1 and 3, respectively. Next, there are four blue square buttons that are used to actuate the resistive loads in Zones 2 and 3 respectively. A button press connects the load to the MVDC bus, and a second button push is needed to turn the load off. The two white round buttons are used to increment (right) and decrement (left), respectively, the power consumed by the 480 VAC Mosebach load in Zone 5. Each button press increments or decrements the load by an amount defined by the user in the LabVIEW virtual instrument (VI) panel, discussed next. Finally, the two large round buttons are used to actuate the 6 kVDC and 12 kVDC power supplies, respectively. The top button commands the 6 kVDC supply to output a 5 second on/ 1 second off pulsed profile into the 6 kVDC Mosebach load. The lower button commands the 12 kVDC supply to output a 5 second on/ 5 second off pulsed profile into the 12 kVDC Mosebach load. Each button press actuates a single instance of its respective load profile, whose power level is set by the user, and holding either button causes the profile to be repeated for as long as it is held.

2.11.3 NI and OPAL-RT Control

A custom DAQ and control system has been written using NI LabVIEW software. The main LabVIEW VI that has been written to interface with the cDAQs is shown in Figure 18. There are many sections that make up the VI. The first, shown in the left blue column, is for controlling the 12 kVDC, 1 kVDC, and 6 kVDC power supplies, respectively. The program gives each of those supplies setpoints as well as their inhibit and enable commands, respectively. Once enabled onto their respective bus, the control box in Figure 16, is used to command them.

Figure 18: Main control VI used to interface and control all the power supplies and loads within the testbed

Moving to the right in the VI, the upper black section is where the MV6000 is controlled. The user is able to set the MV6000's voltage and frequency there when the analog control feature is not being used. There are several other interface commands that are required by the MV6000 for safe operation and those are handled there. Moving down, there is a digital version of the control box that reflects its present state. This is more for user convenience than anything else and for helping to verify that the box is sending the proper commands. Moving down to the orange section in the middle, this is where network variables are received from another VI collecting and recording data from the NI PXI chassis that is monitoring data throughout the testbed. These variables are received by the main VI which then serves as the interface between the hardware and the OPAL-RT. Finally, the rightmost blue column in the VI is where each of the four respective Mosebach loads is controlled. It is here where each respective 50 kW step in the MVDC loads can be added or removed and where the 480 VAC load's step resolution can be set.

There are three separate VIs used to monitor and collect data from the PXI chassis, control the 1 kVDC battery, and monitor data from the battery's BMS, respectively. Those will not be shown in detail here but they are designed to monitor real time data and pass network variables back to the main VI in Figure 18 to be used for autonomous control.

3. Proposed Control Methodology

The intent of the testbed is to use it to study new architectures, new control strategies, and for model validation and verification. Since the testbed has only recently been commissioned, the bulk of the study on control strategies has focused on the virtual extension. To date, the extended model has been kept simple with plans to expand it in the future. This section includes a discussion on applied distributed control and it's use in the IDEAL testbed in tandem with an overarching controller.

3.1.   Multi-agent Formation Control of Generation Sources and Loads

The hardware zone and the extended software zones each have their own loads and generation sources, as described already. The benefit of a zonal architecture is its ability to react to local needs while being able to share power to other zones when critical needs arise that cannot be met within the local zone. Multi-agent formation control is one possible strategy for reliably and efficiently controlling the many different possible sources and loads.

Applying distributed control theory, the generators that are following a reactive and real power trajectory about a load demand, can be equated to multi-agent formation control around a given node. If the real and

reactive power of a load are set as the x and y coordinates on a Cartesian plane, respectively, then any number of generation sources greater than one could be placed on a circle around a shipboard load to source the required power. The circle needs to be defined such that at any arbitrary load value is sourced by the summation of the sources real and reactive power. Should the power supplied by four individual sources be positioned as the corners of a square centered around the load, then their sum would equate to the required load power. An example would be as follows:

$$S_1 = [10\ W\ ; 10\ VAR]$$
$$S_2 = [10\ W\ ; -10\ VAR]$$
$$S_3 = [\ -10W\ ; 10\ VAR]$$
$$S_4 = [-10\ W;\ -10\ VAR]$$

Within each matrix, a positive value represents power being sourced and a negative value represents power being sunk. Inductive sources do not sink power. In the IDEAL scenario being considered here, 'sources' are defined as zones. Since each zone has both sources and loads, power can be both sourced and sunk by an individual zone. The sum of all values in S_i should be equal to that of the load with energy storage being able to absorb any difference. Using multi-agent formation control, where the load is point around which the zone powers are centered, each zone is controlled using equation 1.

$$u_i = cK_p\left[\sum_{j\epsilon N_i} a_{ij}(p_j - \Delta_j - p_i + \Delta_i) + g_i(p_0 - p_i + \Delta_i)\right] + cK_d\left[\sum_{j\epsilon N_i} a_{ij}(q_j - q_i) + g_i(q_0 + q_i)\right]$$

$$(1)\ [18]$$

where Δ_i is the is the offset power from the load, p is the real power, q is the reactive power, a subscript of 0 refers to the load, and a subscript of i refers to one of the ith sources. Here, u_i is the control, or driving force, of the ith node. The exact physical control is determined by the device itself, ie. 0-10 V and would be supplied by the NI controller discussed earlier for example. This control algorithm takes advantage of the relative proximity of the sources to the loads. They can respond accordingly to any load profile or unexpected varying load to more efficiently power the system and create a smoother power transition. Supposing an optimal setpoint is determined based on statistical analysis of what loads are most likely to come on next, that can be used to determine which generators need to be ready. Unexpected loading or unloading of an AC generation source can lead to voltage sags and surges that pull the generation source out of acceptable power quality standards. Maintaining a steady base load ensures the generator can remain within the acceptable bounds. By being able to predict the upcoming load, a software prediction can be used to minimize load changes seen by any individual generator, allowing them to steadily ramp and maintain power quality.

If the output of each AC source is regulated using some form of AC/DC or AC/AC converter, then the formation control algorithm can control the setpoints at each node such that their summation maintains a desired value. This involves controlling the deltas of the formation control. In the testbed, the 480 VAC to 1.2 kVDC converter is used to regulated the AC bus onto the 1 kVDC bus, on which the battery is floated. The 1 kVDC to 6 kVDC converter is used to regulate power to the 6 kVDC load. The output of the battery is indirectly controlled by regulating the power supplied by the AC/DC converter. The current into the DC/DC converter is equal to the sum of that supplied by the AC/DC converter and the battery, respectively, so controlling the AC/DC output current controls the battery's output current. Optimization of many different parameters can be achieved through the regulation of the power from each of these two respective sources. For example, if the AC power quality is to be optimized, the battery current would be regulated such that deviation of the AC source is minimized. If the state of charge (SoC) of the battery is to be optimized, the AC source would be regulated to minimize SoC deviation. These are just two of the many possibilities.

3.2. Time-Varying Graph Topologies

Communication amongst the different zones in a zonal architecture is critical for optimized sharing to be achieved. A communication graph is one way of describing how communication is setup. Intrazonal and interzonal graphs define the communication that occurs within each zone and the communication between zones, respectively. Communication graphs for the IDEAL hardware testbed are shown in Figure 19 and Figure 20, respectively. Figure 19 is drawn to graphically correlate with Figure 2, both in placement and color code, and Figure 20 is drawn to be more clearly visible.
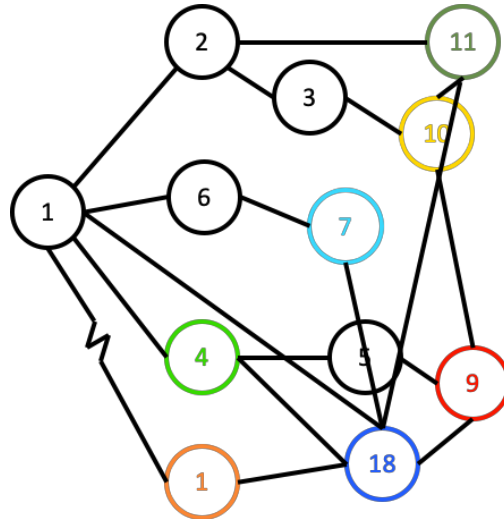
Figure 19: Communication graph for the IDEAL testbed lined corelated to Figure 2.
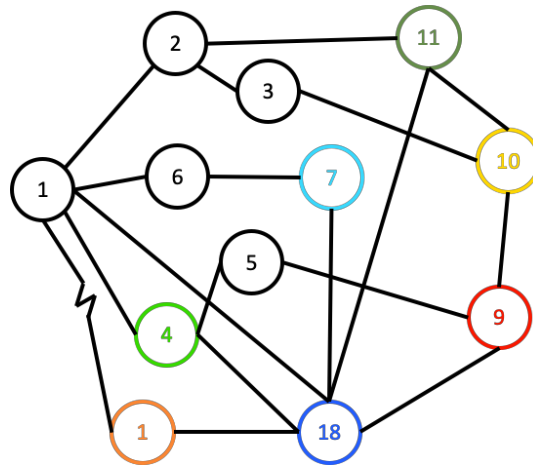
Figure 20: Redrawn Communication graph such that no paths run over a node for easier visualization.

The graphs depict the larger union of the potential time-varying graphs and do not represent the communication at any arbitrary time step. The communication graphs are as dynamic as the loads and sources themselves since nodes can change whom they communicate with and who they receive communications from. For example, when a generation source or load is off, there is limited communication with it. As something comes online, communication with it becomes critical. If a more efficient communication path is identified, the ability to dynamically adjust ensures that communication is optimized. Preventing incorrect or malicious data within the communication path is also critical and security measures must be implemented and dynamically adjusted as needed. Collection and processing of data from the many testbed's many distributed sensors occurs at a discrete sampling rate. Considering this, discrete-time node dynamic system is considered as highlighted in equation 3.

$$x_i(k + 1) = x_i(k) + u_i(k) \qquad (2)$$

These dynamics depend directly on the governing communication graph which is developed from equation 4 [18].

$$F = (I + D)^{-1}(I + A) \qquad (3)$$

In equation 4, I is the N x N identity matrix and D and A are the in-degree and adjaceny matrix of the nodes, respectively. The system dynamics are directly correlated to F. The reader is directed to other sources for more explanation on the contributions of the in-degree, adjacency, and F matrices to the dynamics of a system. The communication topology is potentially changing at each time step and as such, the F matrix can change with k as seen in equation 5.

$$x(k + 1) = F(k)x(k) \qquad (4)$$

The testbed as it exists, currently relies on a limited set of graphs that are controlled by need. The testbed adjusts the edge weights of vital loads to make them more robustly follow each other and removes

communication to the non-vital loads. The removed loads can be adjusted in the control panel itself or prior to control execution. The latter is the defining of the loads to be shed in the event of an overload situation. The application of this control theory to the testbed is still ongoing with results expected soon.

4. Experimental Results

The testbed has been commissioned using manual control and some of those results will be shown here. Beginning with the hardware results, Figure 21 shows a plot of the voltage and current, respectively, measured from the KATO M-G set during the entire experiment is shown. The data shows how the generator is transiently loaded by the pulsed loads. A major goal of the controller is to reduce transient loading of the generator such that any transitions occur via optimized ramp rates that are set by the NI or the OPAL-RT controller, respectively. In the data reported here, the intent is to show the functionality of the testbed and operation of the NI controller. A zoomed in view of the data collected from all the DC sources and loads is shown in Figure 22 and a zoomed in view of all the AC source and load data is shown in Figure 23. Moving from the top down in Figure 22, the first two blue plots show the current and voltage, respectively, from the 1 kV lithium-ion battery that is connected within the branch supplying the 5 s on/ 1 s off 6 kVDC Mosebach load. The voltage and current, respectively, measured at the 6 kVDC PCC are shown in the two red plots. The 5 s on/ 1 s off pulsed profile is repeated as the user presses and holds the upper red button on the control box. Power is sourced into the 6 kVDC supply by both the 1.2 kVDC supply and the battery, respectively. The 1.2 kVDC power supply's current is limited to 15 A by the user within the NI VI using analog voltage control. This is seen in the green plot and except for a few short transients where it deviates, the power supply's current is regulated quite well. During each 5 s on period, during which the load is active, both the battery and the AC generator, who's current is regulated by the 1.2 kVDC supply, source power to the load. During each 1 s off period when the load is inactive, power is sourced by the 1.2 kVDC power supply into the battery, recharging it. This type of operation demonstrates the use of a battery to buffer a transient load sourced by a rotating machine.
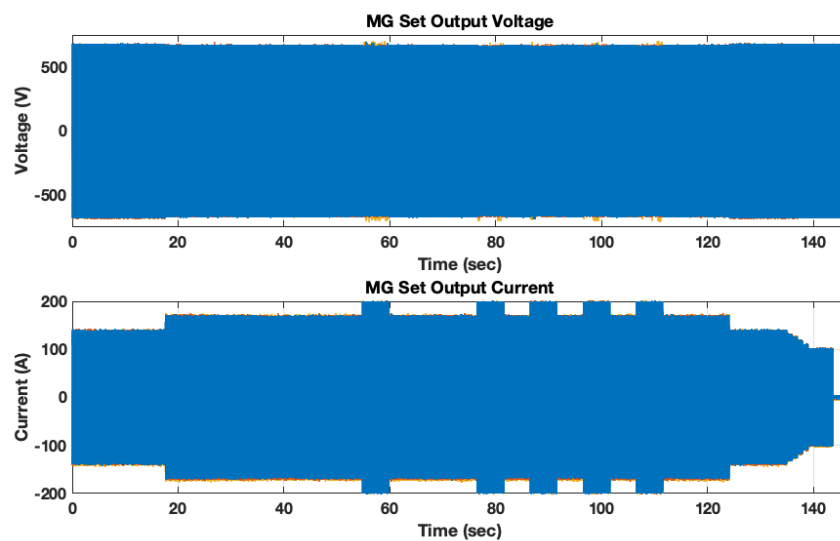
Figure 21: Plot of the current sourced by the KATO M-G set during the full experiment performed.
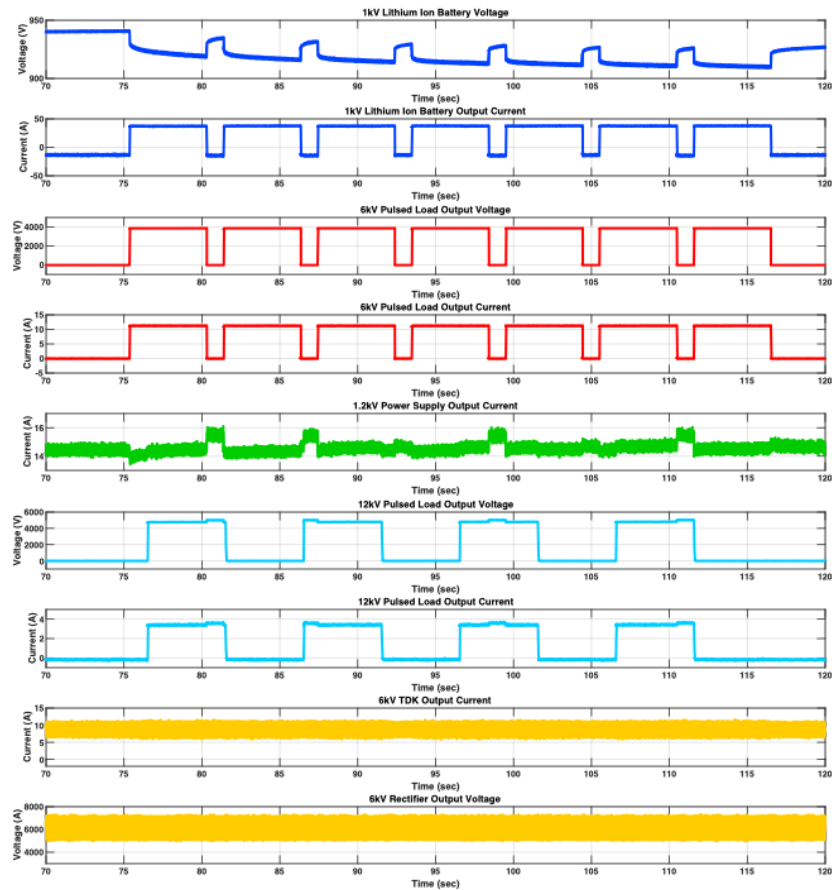
Figure 22: Zoomed in plot of the DC voltages and currents measured within the testbed during a commissioning experiment.

The next two light blue plots in Figure 22 show the voltage and current, respectively, measured on the 12 kVDC bus. A 5 s on/ 5 s off pulsed profile is measured and this is engaged when the user presses and holds the lower red button on the control box. Since this bus is only supplied by the 12 kV power supply, these plots represent its voltage and current, respectively, as well. It should be noticed that the 12 kV is not measured on the 12 kV bus and that is intentional during commissioning. While the power supply and load have been independently verified at voltages as high as 12 kVDC, an abundance of caution was used early in the life of the testbed and it was decided not to operate it that high in this experiment. Since the 12 kV load is a constant resistance, regulation of the 12 kVDC power supply's output current regulates the bus voltage so limiting the current to just under 4 A produces roughly 5 kVDC on the bus. Notice how the 5 s on/ 1 s off and the 5 s on/ 5 s off pulsed profiles, respectively, overlap in some instances and in others only one load is on while the other is in a rest mode. This is what causes many of the sharp transients measured from the AC source data presented in Figure 21. In this experiment nothing is done currently to prevent this type of operation; in the future it can be mitigated in a few different ways. As one example, the 1.2 kVDC supply's setpoint can be actively adjusted by the main VI such that its current is increased to charge the battery at a higher rate during off periods and its current is decreased during on periods such that the battery supplies more of the 6 kVDC load current. This will help to maintain the power supplied by the generator and keep it more constant. Another way to maintain steady operation is shed or bring on load as needed, in this case mostly through the incrementing or decrementing the 480 VAC load setting.

In case the M-G set is loaded beyond its ratings, the controller is designed to respond in a protective manner. Its first course of action is to roll back the current on the 1.2 kV AC/DC supply. If that does not bring the load down sufficiently, the next course of action is to step down the load on the 480 VAC Mosebach load and if that is not enough, then it starts to sequentially bring down all additional loads until safe conditions are met.

In the experiment, the MV6000's voltage level was set to 4160 VAC (1 PU) and its frequency is set to 60 Hz. The last two yellow plots in Figure 22 show the voltage and current, respectively, measured at the output of the 6 kV AC/DC rectifier. The rectifier supplies its own 6 kV constant resistance Mosebach load. Since there is no active control of the rectifier and the MV6000's output current isn't actively regulated; this branch acts as a near

constant baseload for the generator. During this experiment, only one 50 kW load step was actuated in the 6 kVDC load on that bus, and no other changes were made to it throughout the experiment. Notice that there is significant ripple in the output voltage and consequently the output current. That is due to the five-level converter output of the MV6000 and it can be reduced in the future using filters.

A zoomed in view of the AC voltage and current measured from the M-G set and the MV6000, respectively, are plotted in Figure 23. Also plotted is the current measured going into the 4160 VAC to 6 kVDC AC/DC rectifier and the current going into the 4160 VAC to 480 VAC step-down transformer, the latter of which is solved for mathematically by subtracting the former from the MV6000's output current measurement. The output of the transformer, the input to the 480 VAC load, is not measured in the current configuration but that diagnostic will be added in the future. During the experiment, the 480 VAC load was not incremented or decremented for simplicity and only acts as an additional low-level baseload. Within these graphs, the frequency of the hardware sources. The control on this from the software was enforced by feeding in an analog setpoint to the generator and MV6000 to assign the frequency. Together, all these plots show the operation of the testbed, the cumulative loading of all sources, and the control hierarchy that has been developed.
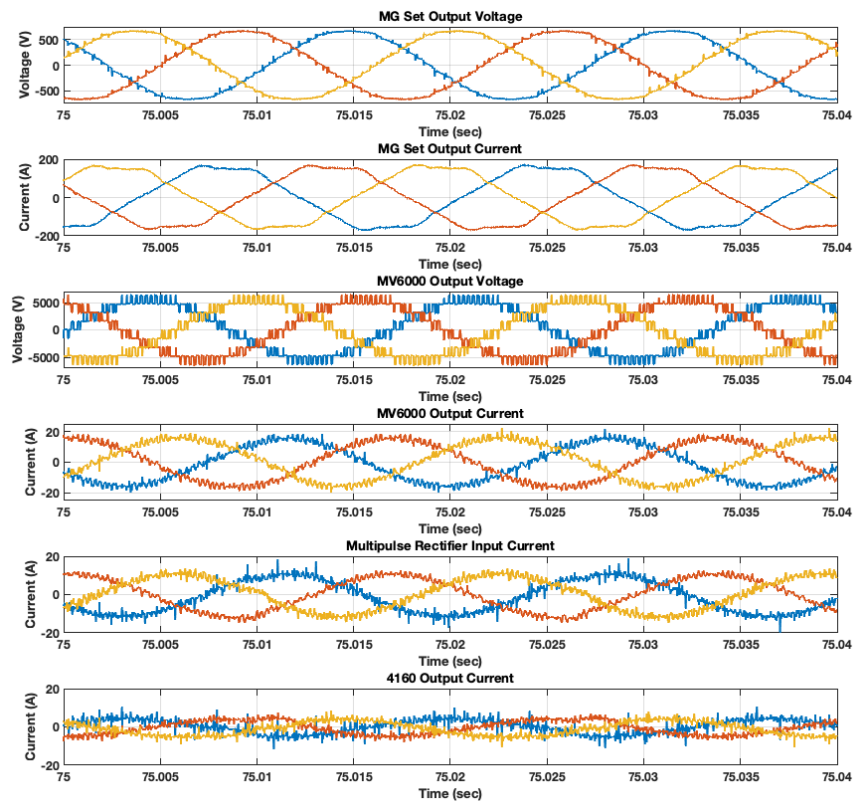
Figure 23: Zoomed in plot of the AC voltages and currents measured within the testbed during a commissioning experiment.

The proposed formation control was tested on a few zones of the software model. A few of the simplified zones were centred around an aggregate load profile. As shown in earlier discussion, the generators are targeted around a square around the changing load profile.

$$S_1 = [10\,;10]$$
$$S_2 = [10\,;-10]$$
$$S_3 = [\,-10\,;10]$$
$$S_4 = [-10\,;\,-10]$$

For the purpose of demonstration, an arbitrary load profile was used. The path linearly rose and was added to a small oscillation to model a changing load. As can be seen in Figure 25, the generation sources first spread out to reach the desired formation, then rigidly follow with the path of the load.
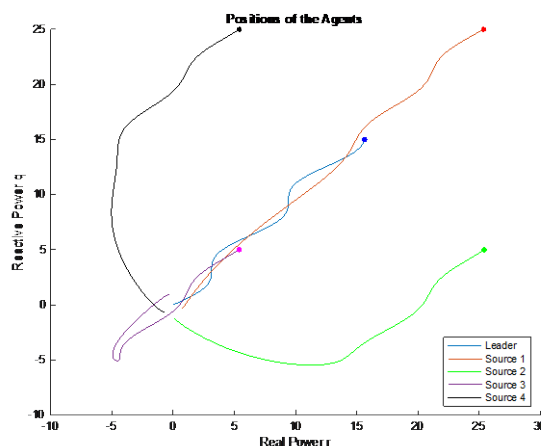
Figure 24: Formation control of the active and reactive power of four generation sources around an aggregate load.

5. Conclusions

In this report, the design, construction, and commissioning of the UTA **I**ntelligent **D**istributed **E**nergy **A**nalysis **L**aboratory (IDEAL) has been presented along with several opportunities for the implementation of distributed control systems in zonal shipboard architectures. The testbed was designed as a platform on which the integration and controls challenges that future shipboard distributed power system engineers will face can be studied and better understood. Significant challenges exist in integrating distributed generation and transient loads and it is anticipated that the testbed will be invaluable to identifying and overcoming them. The testbed, operating at power levels in the few hundred kW range, utilizes distributed AC and DC power sources and loads operating at the 480 VAC, 4160 VAC, 1 kVDC, 6 kVDC, and 12 kVDC, respectively. The testbed is being extended utilizing an OPAL-RT HIL simulator and automated formation control to further test and validate the shipboard power systems. To date, all the hardware has been installed and it has been commissioned using the NI controller that has been developed. It has been extended to a five zone power system using a very simple shipboard model. There is still much work to be done but a foundation has been laid.

Acknowledgements

References

[1]   N. Doerry and J. Amy, 'MVDC Shipboard Power System Considerations for Electromagnetic Railguns,' 6th DOD Electromagnetic Railgun Workshop, Laurel, MD, September 2017.

[2]   J. Thongam, et al. "All-electric ships—A review of the present state of the art," 8th International Conference and Exhibition on Ecological Vehicles and Renewable Energies, pp. 1-8, March 2013.

[3]   Next Generation Integrated Power System, NGIPS Technology Development Roadmap, Ser 05D / 349, November 30, 2007.

[4]   Office of Naval Research. "Hybrid Energy Storage Module (HESM): Amendment 001" 13-SN-0007 [Online]. Available: http://www.onr.navy.mil/~/media/Files/Funding-Announcements/Special-Notice/2013/13-SN-0007-Amendment-0001.ashx.

[5]   I.J. Cohen, J.P. Kelley, **D.A. Wetz**, and J.M Heinzel, 'Impact of a Hybrid Energy Storage Module on the Power Quality of a Fossil Fuel Generator within a MicroGrid,' *Naval Engineers Journal,* Vol. 129, No. 1, March 2017, pp. 147 – 155.

[6]   D.N. Wong, A.M. Mansour, D.A. Wetz, and J.M. Heinzel, 'Characterizing Rapid Capacity Fade and Impedance Evolution in High Rate Pulsed Discharged Lithium Iron Phosphate Cells for Complex, High Power Loads,' Volume 328, 1 October 2016, Pages 81 – 90.

[7]   N. Doerry and J. Amy, 'MVDC Shipboard Power System Considerations for Electromagnetic Railguns,' 6th DOD Electromagnetic Railgun Workshop, Laurel, MD, September 2017.

[8] D.A. Wetz, P.M. Novak, B. Shrestha, J.M. Heinzel, and S.T. Donahue, 'Electrochemical Energy Storage Devices in Pulsed Power,' IEEE Transactions on Plasma Science, Vol. 42, No. 10, Part 2, pp. 3034 – 3042, October 2014.

[9] D.A. Wetz, B. Shrestha, and P.M. Novak, 'Pulsed Evaluation of High Power Electrochemical Energy Storage Devices,' IEEE Transactions on Dielectrics and Electrical Insulation, Vol. 20, No. 4, pp. 1040 – 1048, August 2013.

[10] D.A. Dodson, D.A. Wetz, J.L. Sanchez, C.G. Gnegy-Davidson, M.J. Martin, B. Adams, A.N. Johnston, J.M. Heinzel, S. Cummings, N. Frank, N.A. Rahim, and M. Davis, 'Design and Evaluation of a 1000 V Lithium-Ion Battery,' *Naval Engineers Journal,* Vol. 131, No. 3, September 2019, pp. 107 – 119.

[11] D.A. Wetz, M.J. Martin, C.L. Williams, K.D. Mckinzie, I.J. Cohen, C.G. Gnegy-Davidson, and J.M. Heinzel, Design of 1000 V Valve Regulated Lead Acid (VRLA) and Lithium-Iron-Phosphate Lithium-Ion (LFP-LI) Battery Test Beds for Driving High Rate, Pulsed Loads, Proceedings of the 2016 Advanced Machinery Technology Symposium (AMTS), May 25 – 26, 2016, Philadelphia, Pennsylvania.

[12] I. Cohen, D.A. Wetz, Q. Dong, J.M. Heinzel, and S. Veiga, 'Fuzzy Logic Control of a Hybrid Energy Storage Module for System Level Control of COTS Components Driving Pulsed Loads,' International Journal of Fuzzy Logic Systems (IJFLS) Vol.6, No.1, January 2016.

[13] I.J. Cohen, J.P. Kelley, D.A. Wetz, and J. Heinzel, 'Evaluation of a Hybrid Energy Storage Module (HESM) for Pulsed Power Applications,' IEEE Transactions on Plasma Science, Vol. 42, No. 10, Part 2, pp. 2948 – 2955, October 2014.

[14] J.L. Sanchez, D.A. Wetz, and Q. Dong, and J.M. Heinzel, 'Integration and Study of Hardware in the Loop Diesel Generator with a Hybrid Energy Storage Module for Naval Applications,' Proceedings of the 2017 IEEE Electric Ship Technologies Symposium (ESTS), August 15 – 17, 2017, Crystal City, Virginia, pp. 580 – 585. (Oral Presentation)

[15] GE Power Conversion, 'MV6 Medium Voltage Drive - Leading next generation technology,' https://www.gepowerconversion.com/sites/default/files/GEA30738C%20MV6%20Medium%20Voltage%20Drive.pdf, [ONLINE], Copyright © 2014 General Electric Company and/or its affiliates.

[16] R. H. Lasseter et al., "CERTS Microgrid Laboratory Test Bed," in IEEE Transactions on Power Delivery, vol. 26, no. 1, pp. 325-332, Jan. 2011, doi: 10.1109/TPWRD.2010.2051819.

[17] M. Saleh, Y. Esa, Y. Mhandi, W. Brandauer and A. Mohamed, "Design and implementation of CCNY DC microgrid testbed," 2016 IEEE Industry Applications Society Annual Meeting, Portland, OR, 2016, pp. 1-7, doi: 10.1109/IAS.2016.7731870.

[18] B.J. McRee, D.A. Dodson, D.A. Wetz, and A.N. Johnston, 'Utilization of Power Hardware-in-the-Loop to Study Power Conversion Topologies and Control in Distributed Generation Power Systems,' Proceedings of the 2019 IEEE Electric Ship Technologies Symposium (ESTS), August 14 – 17, 2019, Arlington, Virginia. (Poster Presentation)

[19] ODiSI, Luna Innovations Inc., http://lunainc.com/odisi, [ONLINE], March 20, 2018, © 2018, Luna.

[20] F. L. Lewis, Kristian Hengster-Movric, Hongwei Zhang, and Abhijit Dasgupta, *Cooperative Control of Multi-Agent Systems,* Springer-Verlag London 2014.